

See discussions, stats, and author profiles for this publication at: <https://www.researchgate.net/publication/283851719>

Surfactant modulated aggregation induced enhancement of emission (AIEE) — a simple demonstration to maximize sensor activity

ARTICLE *in* THE ANALYST · NOVEMBER 2015

Impact Factor: 4.11 · DOI: 10.1039/C5AN01916H

READS

79

5 AUTHORS, INCLUDING:



Rahul Bhowmick

Jadavpur University

8 PUBLICATIONS 6 CITATIONS

[SEE PROFILE](#)



Atul Katarkar

Indian Institute of Chemical Biology

23 PUBLICATIONS 21 CITATIONS

[SEE PROFILE](#)



Keya Chaudhuri

Indian Institute of Chemical Biology

157 PUBLICATIONS 1,745 CITATIONS

[SEE PROFILE](#)



Mohammad Ali

Jadavpur University

119 PUBLICATIONS 795 CITATIONS

[SEE PROFILE](#)



Cite this: DOI: 10.1039/c5an01916h

Surfactant modulated aggregation induced enhancement of emission (AIEE)—a simple demonstration to maximize sensor activity†

Rahul Bhowmick,^a Abu Saleh Musha Islam,^a Atul Katarkar,^b Keya Chaudhuri^b and Mohammad Ali*^a

A new type of easily synthesized rhodamine-based chemosensor L^3 , with potential NO_2 donor atoms, selectively and rapidly recognizes Hg^{2+} ions in the presence of all biologically relevant metal ions and toxic heavy metals. A very low detection limit (78 nM) along with cytoplasmic cell imaging applications with no or negligible cytotoxicity indicate good potential for *in vitro/in vivo* cell imaging studies. SEM and TEM studies reveal strongly agglomerated aggregations in the presence of 5 mM SDS which turn into isolated core shell microstructures in the presence of 9 mM SDS. The presence of SDS causes an enhanced quantum yield (ϕ) and stability constant (K_f) compared to those in the absence of SDS. Again, the FI of the $[\text{L}^3-\text{Hg}]^{2+}$ complex in an aqueous SDS (9 mM) medium is unprecedentedly enhanced (~143 fold) compared to that in the absence of SDS. All of these observations clearly manifest in the enhanced rigidity of the $[\text{L}^3-\text{Hg}]^{2+}$ species in the micro-heterogeneous environment significantly restricting its dynamic movements. This phenomenon may be ascribed as an aggregation induced emission enhancement (AIEE). The fluorescence anisotropy assumes a maximum at 5 mM SDS due to strong trapping (sandwiching) of the doubly positively charged $[\text{L}^3-\text{Hg}]^{2+}$ complex between two co-facial laminar microstructures of SDS under pre-micelle conditions where there is a strong electrostatic interaction that causes an improved inhibition to dynamic movement of the probe-mercury complex. On increasing the SDS concentration there is a phase transition in the SDS microstructures and micellization starts to prevail at SDS ≥ 7.0 mM. The doubly positively charged $[\text{L}^3-\text{Hg}]^{2+}$ complex is trapped inside the hydrophobic inner core of the micelle which is apparent from the failure to quench the fluorescence of the complex on adding 10 equivalents of $\text{H}_2\text{EDTA}^{2-}$ solution but in the absence of SDS it is quenched effectively.

Received 16th September 2015,
Accepted 5th November 2015

DOI: 10.1039/c5an01916h
www.rsc.org/analyst

Introduction

In the nature, there is a continuous drive of a web of chemical reactions of elements, ions and molecules.¹ Living organisms and their environment interact with each other through a diverse array of reactions spanning from covalent to non-covalent interactions like electrostatic, hydrophobic, van der Waals, hydrogen bonding *etc.*^{2,3} and significant progress in the design and fabrication of appealing supramolecular assemblies has been achieved by chemists through bottom-up approaches by elegant utilization of these non-covalent inter-

actions, which led to the successful fabrication of optical materials and advanced nano-devices. It involves coupling of structurally different building blocks (ionic pairs) by electrostatic interactions.³ Various combinations between polyelectrolytes, peptides, surfactants and extended rigid organic scaffolds could be employed for creating new material *via* ionic self-assembly.^{4–9} Another promising feature of these supramolecular assemblies concerns their emissive behavior in solution and solid states. The assemblies formed thereof may exhibit either aggregation caused quenching (ACQ) or aggregation induced emission enhancement (AIE or AIEE);^{10–17} the latter shows enhanced fluorescence emission efficiency in an aggregated state as compared to that in a solution state. In this context, the AIEE phenomenon became a key point in developing materials for fluorescent sensors, optoelectronic devices, and cell imaging applications. Up to now, the AIEE mechanism has been observed in silole derivatives,¹⁸ 1,1,2,2-tetraphenylethene (TPE),^{19–22} and 1-cyano-*trans*-1,2-bis-(4-methylphenyl) ethylene (CN-MBE),^{23,24} which were claimed to be stimuli responsive

^aDepartment of Chemistry, Jadavpur University, 188, Raja Subodh Chandra Mallick Rd, Kolkata, West Bengal 700032, India. E-mail: m_ali2062@yahoo.com

^bDepartment of Molecular & Human Genetics Division, CSIR-Indian Institute of Chemical Biology, 4 Raja S.C. Mallick Road, Kolkata-700032, India

† Electronic supplementary information (ESI) available: Synthesis and corresponding characterization data for compound L^3 . See DOI: 10.1039/c5an01916h

materials capable of detecting volatile organic vapor, biological polymers, pH changes, explosives, metal ions *etc.*

Fluorescence efficiency greatly depends on a number of factors that maximize the stability of a fluorophore in the excited state and minimize various non-radiative decay processes such as intermolecular interaction,²⁵ intramolecular charge transfer,^{26,27} and intramolecular torsional and rotational motions.^{28–30} One of the ways to achieve this is to confine a probe by changing the outside environment which significantly deactivates these non-radiative decay processes and enhances the fluorescence efficiency – a way to develop organic light-emitting diodes for practical applications.^{31,32} Thus, a number of fluorescent molecules exhibit aggregation-induced emission (AIE) properties by restricting the intramolecular vibrational, rotational, and torsional motion resulting in a turned on or enhanced fluorescence.³³ An obvious choice is to use ionic surfactants where electrostatic interactions with a charged fluorescent probe suppress the non-radiative decay and hence enhance the fluorescence emission efficiency. Surfactants generally form micelles, vesicles, and other kinds of aggregates,³⁴ and therefore could be a good choice to modulate the aggregation of ionic fluorescent dyes in water and to adjust the fluorescence intensity. All of these have found applications in biochemistry, analytical chemistry, and photosensitization.^{35–37} However, only a few reports are available where induced fluorescence enhancement of dye molecules by surfactants occurs.^{38–42}

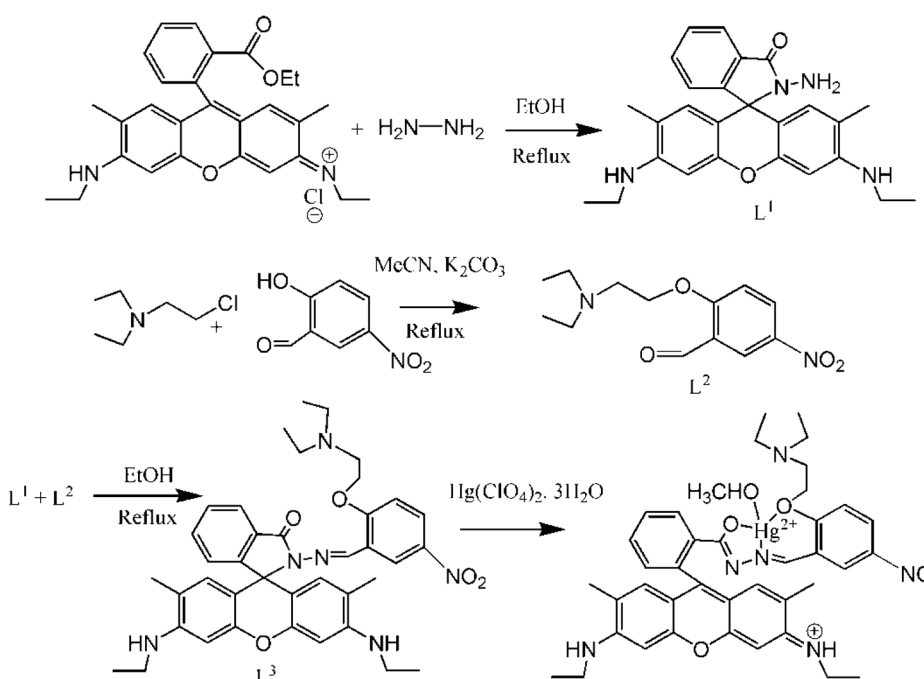
Again, pollution due to heavy metals like mercury arises due to their wide scale applications in agriculture and industry. It is also widespread in air, water and soil by oceanic and

volcanic eruptions, combustion of fossil fuels, gold mining and solid waste incineration and seems to be inescapable.^{43–45} An example of a highly toxic and widespread pollutant is the water-soluble Hg²⁺ ion, which can damage the brain, nervous system, kidneys, and endocrine system. In living organisms Hg²⁺ deactivates many enzymes due to its strong affinity for sulfur in -SH groups which stops or alters metabolic processes.^{46,47} As a result of the accumulation of Hg²⁺ in the body, various diseases like prenatal brain damage, serious cognitive and motion disorders, Minamata *etc.* are common.⁴⁸

There are several sophisticated analytical instruments like atomic absorption and emission spectroscopy,⁴⁹ inductively coupled plasma mass spectroscopy (ICP-MS),⁵⁰ inductively coupled plasma atomic emission spectrometry (ICP-AES),⁵¹ voltammetry⁵² *etc.* which are used for Hg²⁺ detection, however, most of these methods are either very costly or time-consuming and not suitable for performing assays. However, quick response times, high sensitivity and good selectivity make the fluorescence technique superior to others and has attracted tremendous attention from chemists, biologists and environmentalists.^{53–59}

Special structural features along with good photostability, a high molar extinction coefficient and a longer emission wavelength (550 nm) make rhodamine a good choice for the construction of OFF-ON fluorescent chemosensors⁵¹ to avoid background fluorescence below 500 nm.^{53,57,60}

Here, a new rhodamine-based probe with potential NO₂ donor atoms has been synthesized and successfully employed for the selective and rapid recognition of toxic Hg²⁺ ions (Scheme 1) in a 8 : 2 (H₂O : MeCN) medium. It exhibits very



Scheme 1

rapid chromo- and fluorogenic OFF-ON responses through metal-induced opening of the spirolactam ring. Not only that, in aqueous SDS medium, it was found to exhibit aggregation induced emission enhancement (AIEE).

Experimental section

Materials and instruments

Rhodamine 6G hydrochloride, 2-chloro-*N,N*-diethylethylamine hydrochloride and metal salts such as perchlorates of Na^+ , K^+ , Ca^{2+} , Fe^{2+} , Co^{2+} , Ni^{2+} , Zn^{2+} , Pb^{2+} , Cd^{2+} , Hg^{2+} and Cu^{2+} and anions such as SO_4^{2-} , NO_3^- , PO_4^{3-} , S^{2-} , Cl^- , F^- , Br^- , OAc^- , H_2AsO_4^- , N_3^- , ClO_4^- , PPi , $\text{S}_2\text{O}_4^{2-}$, HCO_3^- , SCN^- , CO_3^{2-} , $\text{P}_2\text{O}_7^{4-}$ and NO_2^- were purchased from Sigma-Aldrich and used as received. All solvents used for synthetic purposes were of reagent grade (Merck) unless otherwise mentioned. For spectroscopy (UV/Vis and fluorescence) studies HPLC-grade MeCN and deionized water from MiliQ Millipore were used.

UV/Vis absorption spectra were recorded on an Agilent 8453 diode array spectrophotometer. Steady-state fluorescence studies were carried out with a PTI (QM-40) spectrofluorimeter. NMR spectra were recorded on a Bruker spectrometer at 300 MHz. The ESI-MS⁺ spectra were recorded on a Waters XEVO G2QToF mass spectrometer.

Preparation of Rhodamine 6G hydrazide (L^1)

Rhodamine-6G hydrazide was prepared according to a method in the literature.⁶¹

Preparation of 2-[2-(diethylamino)-ethoxy]-5-nitro-benzaldehyde (L^2)

In a typical procedure 5-nitro salicylaldehyde (5 mmol, 0.835 g) was dissolved in dry MeCN (30 mL) to which K_2CO_3 (6 mmol, 0.3312 g) was added, and the mixture was heated at reflux for 40 min. 2-Chloro-*N,N*-diethylethylamine hydrochloride (6 mmol, 1.032 g) was then added and reflux was continued for another 5 h. It was then cooled to room temperature and filtered. The filtrate was evaporated to one third of its initial volume and diluted with 40 mL water. The pH of the resulting solution was then adjusted to 4 by the addition of 1 M HCl and extracted with dichloromethane (DCM; 2 × 40 mL). The pH of the aqueous solution was further adjusted to 8 by the addition of 4.0 M Na_2CO_3 solution and again extracted with DCM (3 × 40 mL). The combined organic phase was dried over anhydrous Na_2SO_4 and then evaporated to dryness under reduced pressure to yield a reddish yellow solid. The solid product was recrystallized from MeCN/DCM (8 : 2, v/v) to give L^2 as an amorphous solid.

Preparation of L^3

2-[2-(Diethylamino)-ethoxy]-5-nitro-benzaldehyde (L^2) (1.10 mmol, 0.266 g) in MeOH (10 mL) was added dropwise to a methanolic solution (30 mL) of L^1 (1 mmol, 0.464 g) containing 1 drop of acetic acid under hot (50–60 °C) conditions over 30 min and was then stirred for about 6 h at room temperature

whereupon a yellow precipitate formed and was collected by filtration. The residue was washed thoroughly with cold methanol to isolate L^3 in pure form at 78% yield. The detailed synthetic steps are illustrated in Scheme 1.

Analysis

¹H NMR (DMSO-*d*₆): δ = 8.83 (s, 1 H), 8.31 (s, 1 H), 8.04 (s, 1 H), 7.92 (s, 1 H), 7.58 (m, 2 H), 7.03 (d, 1 H), 6.92 (d, 1 H), 6.30 (s, 2 H), 6.16 (s, 2 H), 5.07 (t, 2 H), 3.11 (t, 4 H), 2.48 (s, 14 H), 1.82 (s, 6 H), 1.18 (t, 6 H) ppm (Fig. S1†). IR: $\tilde{\nu}$ = 1722 cm⁻¹ (spirolactam amide-keto), 1622 cm⁻¹ (-C=N) (Fig. S2†). MS (ES⁺): *m/z* = 677.4009 [L + H⁺] (Fig. S3†).

Preparation of complex $\text{L}^3\text{-Hg}^{2+}$

$\text{Hg}(\text{ClO}_4)_2$ (0.272 g, 0.6 mmol) was added to a 10 mL MeCN solution of L^3 (0.338 g, 0.5 mmol) and the mixture was stirred for about 30 minutes. It was then filtered and allowed to evaporate slowly at ambient temperature to obtain the crystalline solid product.

Analysis: ¹H NMR (DMSO-*d*₆): δ = 8.83 (s, 1 H), 8.29 (d, 1 H), 8.05 (d, 1 H), 8.03 (d, 1 H), 7.60 (m, 2 H), 7.03 (d, 1 H), 6.92 (d, 1 H), 6.35 (s, 2 H), 6.18 (s, 2 H), 5.45 (s, 1 H), 3.12 (m, 4 H), 2.48 (s, 14 H), 1.83 (s, 6 H), 1.18 (t, 6 H) ppm (Fig. S4†). IR: $\tilde{\nu}$ = 1633 cm⁻¹ (spirolactam ring open), 1608 cm⁻¹ (-C=N) (Fig. S2†). MS (ES⁺): *m/z* = 532.5052 (L^3 + Hg^{2+} + ClO_4^- + H_2O + CH_3OH + CH_3CN) and 629.4355 (L^3 + Hg^{2+} + $(\text{ClO}_4)_3$ + $(\text{H}_2\text{O})_3$ + Li_2) (Fig. S5†).

Solution preparation for UV-Vis and fluorescence studies

For both UV-Vis and fluorescence studies, a 1.0×10^{-3} M stock solution of L^3 was prepared by dissolving the required amount of ligand in 2 mL MeCN and finally the volume was adjusted to 10 mL by deionized water. In a similar way, a 1.0×10^{-3} M stock solution of Hg^{2+} was prepared in deionised H_2O . A 250 mL 10 mM HEPES buffer solution in 8 : 2 H_2O : MeCN (v/v) was prepared and pH was adjusted to 7.2 using HCl and NaOH. 2.5 mL of this buffer solution was pipetted out into a cuvette to which the required volume of the 1.0×10^{-3} M probe was added to achieve 20 μM and 10 μM final concentrations for UV-Vis and fluorescence titration, respectively. At a regular interval a volume of Hg^{2+} ions was added incrementally and UV-Vis and fluorescence spectra were recorded for each solution. Cuvettes with a 1 cm path length were used for absorption and emission studies. Fluorescence measurements were performed using a 2 nm × 2 nm slit width.

Preparation of samples for SEM and TEM studies

We prepared 10 mL 1 mM stock solution of the ligand and 10 mL 0.10 M stock solution of SDS. Now, 25 μL of the ligand solution was added to (a) 125 μL and (b) 225 μL SDS solution in 2.5 mL deionized water with stirring for 5 minutes. The concentrations of SDS/ L^3 in the resulting solutions were (a) 5.0/0.10 mM and (b) 9.0/0.10 mM respectively. The use of higher concentrations of SDS (up to 20 mM) does not show any formation of microstructures. We have prepared another set of solutions (a) and (b) with an appropriate amount of ligand (25 μL)

and to each solution 1 equivalent of Hg^{2+} was added. All of the solutions were aged overnight at room temperature before characterization. The samples in both cases were found to give the best microstructure as analyzed using SEM and TEM.

Methods of characterization

The morphologies of the synthesized nano/microstructures were studied using scanning electron microscopy (SEM) with a ZEOL, JSM 8360 operated at an accelerating voltage of 5 kV. Before SEM studies, the samples were vacuum dried on a glass plate and deposited as a thin layer of carbon. Transmission electron microscopy (TEM) studies were performed on a JEOL JEM 2100 HR with EELS operating between accelerating voltages of 80 kV to 200 kV. The sample was deposited on a copper grid and vacuum dried.

Steady-state fluorescence and fluorescence anisotropy were measured with a PTI QM-40 spectrofluorometer. Fluorescence anisotropy (r) is defined as:

$$r = (I_{VV} - GI_{VH}) / (I_{VV} + 2GI_{VH}) \quad (1)$$

where I_{VV} and I_{VH} are the emission intensities obtained with the excitation polarizer oriented vertically and emission polarizer vertically and horizontally, respectively. The G factor is defined as:⁵³

$$G = I_{HV}/I_{HH} \quad (2)$$

where the intensities I_{HV} and I_{HH} refer to the vertical and horizontal positions of the emission polarizer, with the excitation polarizer oriented horizontally.

Cell culture

Human hepatocellular liver carcinoma (HepG2) cell lines were procured from NCCS (Pune). The cells were cultured in DMEM (penicillin-100 $\mu\text{g ml}^{-1}$, 10% FBS, streptomycin-50 $\mu\text{g ml}^{-1}$) at 37 °C in a 95% air and 5% CO_2 incubator.

Cell viability assay

To determine % cell viability, a colorimetric MTT assay of ligand L^3 was performed by a method reported earlier.⁶²

Cell imaging study

1×10^5 cells were cultured and incubated on a coverslip in a 35 × 10 mm culture dish for 24 h at 37 °C. The cells were treated with 10 μM L^3 (prepared by dissolving L^3 in a mixed solvent of DMSO : water = 1 : 9 v/v) and were then allowed to incubate for 45 min at 37 °C. After incubation cells were incubated with MitoTracker® Green FM (Invitrogen) for 30 min to track the cytoplasm followed by washing thrice with 1× PBS. The cells were then counterstained by DAPI (2-(4-amidinophenyl)-6-indolecarbamidine dihydrochloride, 4',6-diamidino-2-phenylindole, used for nuclear staining, Sigma). Fluorescence images of HepG2 cells were taken using a fluorescence microscope (Leica DM3000, Germany) with an objective lens of 40× magnification. Additionally, fluorescence images of HepG2 cells were taken where cells were pre-incubated with 2 μM , 4 μM ,

8 μM , 16 μM , or 20 μM Hg^{2+} for 3 h in three different culture dishes at 37 °C followed by washing thrice with 1× PBS and then incubated with an equimolar amount of ligand L^3 (2 μM , 4 μM , 8 μM , 16 μM , or 20 μM respectively) for 30 min at 37 °C. After incubation, cells were washed with 1× PBS three times and fluorescence images were taken. L^3 shows intracellular cytoplasmic red fluorescence by forming a complex with Hg^{2+} against the nuclear counterstain DAPI (blue color) and cytoplasmic stain MitoTracker Green (green color).

Results and discussion

A Schiff base condensation between L^1 and L^2 in methanol (Scheme 1) under refluxing conditions yields L^3 , which was thoroughly characterized by $^1\text{H-NMR}$, IR and ESI-MS⁺ spectroscopy.

Absorption and steady-state emission studies

UV-Vis titration with a fixed concentration of L^3 (20 μM) and variable concentrations of Hg^{2+} (0–25.0 μM) at 25 °C in aqueous MeCN (8 : 2, v/v, HEPES buffer, pH 7.2) showed a gradual development of a new absorption band around 533 nm on addition of Hg^{2+} (Fig. 1a).

A plot of absorbance vs. $[\text{Hg}^{2+}]$ gives a non-linear curve (Fig. 1b) with decreasing slope and can be analyzed using eqn (3)⁶³ below. The binding constant of the formed $\text{L}^3-\text{Hg}^{2+}$ complex was determined to be $K_f = (2.39 \pm 0.49) \times 10^4 \text{ M}^{-1}$.

$$y = \frac{a + bx^n}{1 + cx^n} \quad (3)$$

where a = absorption minimum (A_{\min}), b = absorption maximum (A_{\max}) and $c = K_f$ = apparent formation constant.

Job's method was employed to determine the composition of the complex which was found to be 1 : 1 (Fig. 1c). The emission spectra of L^3 and its fluorescence titration with Hg^{2+} were performed in water : MeCN (8 : 2, v/v) solution with a fixed concentration of L^3 (10 μM) (10 mM HEPES buffer, pH 7.2; Fig. 2). On gradual addition of Hg^{2+} (0–56.0 μM) to the non-fluorescent solution of L^3 (10.0 μM), a 316-fold enhancement in fluorescence intensity at 553 nm was observed following excitation at 510 nm, which also suggests an opening of the spiro-lactam ring in L^3 on coordination to the Hg^{2+} ion.

A plot of FI vs. $[\text{Hg}^{2+}]$ gives a straight line up to 50 μM where eqn (3) becomes $y = a + b \times c \times x$ under the conditions $1 \gg c \times x$ and the linear dependence of such a plot gives a slope = $b \times c$, where b = fluorescence maximum (F_{\max}) and $c = K_f$ = apparent formation constant. So, slope/ F_{\max} gives $K_f = (2.02 \pm 0.03) \times 10^4 \text{ M}^{-1}$. It is interesting to note that the values of K_f obtained separately from absorbance and fluorescence titrations are very close to each other and clearly indicate the internal consistency of our results.

The detection of Hg^{2+} was not affected by the presence of biologically abundant metal ions like Na^+ , K^+ , Ca^{2+} and Mg^{2+} . Likewise, under identical reaction conditions no significant color or spectral change was observed for transition-metal

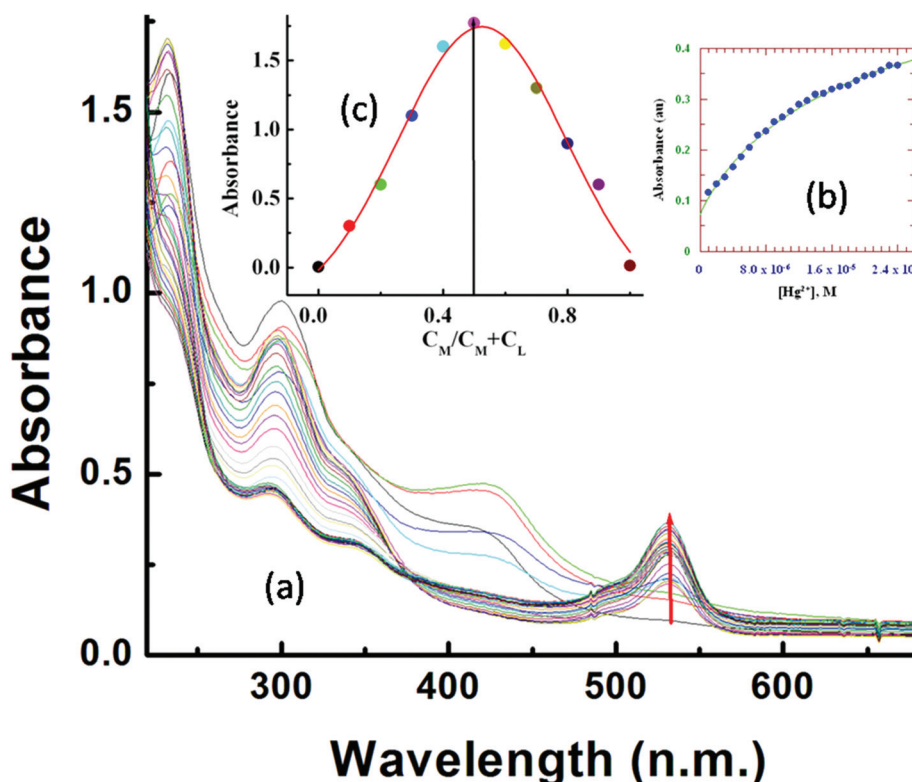


Fig. 1 (a) Absorption titration of L^3 (20.0 μ M) with Hg^{2+} in MeCN–H₂O (2 : 8, v/v) in HEPES buffer (10 mM) at pH 7.2; (b) Non-linear fit of absorbance vs. $[Hg^{2+}]$ plot at $\lambda = 533$ nm; (c) Job's plot for the determination of the composition of the L^3 – Hg^{2+} complex.

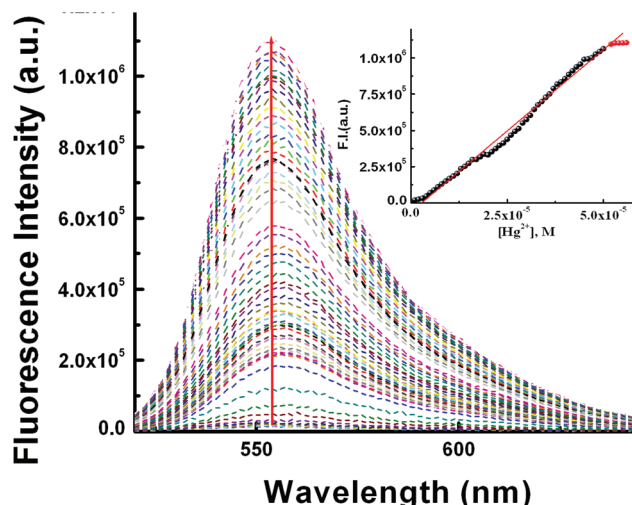


Fig. 2 Fluorescence titration of L^3 (10.0 μ M) in MeCN–H₂O (2 : 8, v/v) in HEPES buffer at pH 7.2 by the gradual addition of Hg^{2+} with $\lambda_{ex} = 510$ nm and $\lambda_{em} = 553$ nm. Inset: linear fit plot of FI vs. $[Hg^{2+}]$.

ions, namely Cr^{3+} , Mn^{2+} , Fe^{2+} , Fe^{3+} , Co^{2+} , Cu^{2+} , Ni^{2+} and Zn^{2+} , and heavy-metal ions, like Cd^{2+} and Pb^{2+} and also anions like SO_4^{2-} , NO_3^- , PO_4^{3-} , S^{2-} , Cl^- , F^- , Br^- , OAc^- , $H_2AsO_4^{4-}$, N_3^- , ClO_4^- , PPI , $S_2O_4^{2-}$, HCO_3^- , SCN^- , CO_3^{2-} , $P_2O_7^{4-}$ and NO_2^- (Fig. 3).

We have also checked the thiophilicity of Hg^{2+} ions using cysteine under extracellular conditions. It was observed that the probe undergoes complete fluorescence quenching on addition of thiol (10 μ M) to an ensemble of 10 μ M L^3 – Hg^{2+} . This clearly indicates that the probe could be used to detect Hg^{2+} as well as thiols to a concentration of at least 10 μ M which are best viewed in Fig. S6.† The quantum yield (ϕ) of the free ligand and the L^3 – Hg^{2+} complex in pure water in the absence and presence of 9 mM SDS were determined and were found to be: 0.0029 (L^3), 0.11 (L^3 in the presence of 9 mM SDS), 0.009 (L^3 in the presence of 1.2 equivalents of Hg^{2+}) and 0.48 (L^3 + 9 mM SDS + 1.2 equivalents of Hg^{2+} in pure water). The lifetime of the free ligand in the absence and presence of SDS (9 mM) is 0.41 and 3.33 ns, respectively, while that of the L^3 – Hg^{2+} complex is 4.51 and 3.31 ns, respectively.

pH stability check

The pH-titration over a wide range of pH (2–12) reveals no obvious fluorescence emission of L^3 between pH 4 and 12. However in the presence of Hg^{2+} it becomes fluorescent between pH 6.5–12 suggesting a convenient application of this probe under physiological conditions (Fig. 4).

Determination of LOD

The 3σ method was adopted to determine the limit of detection (LOD) of Hg^{2+} and it was found to be as low as 78 nM

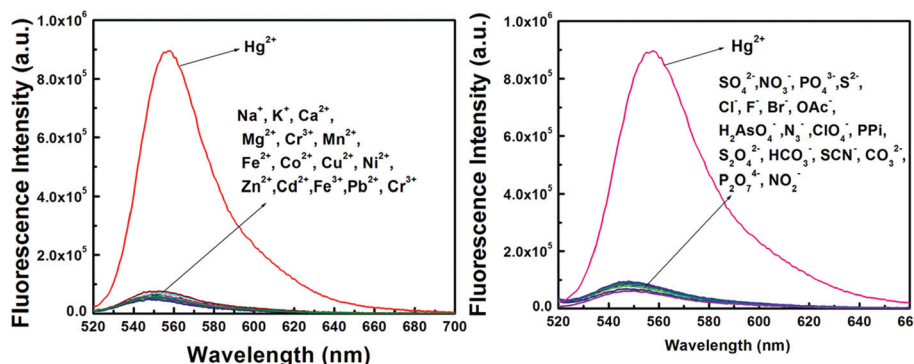


Fig. 3 Fluorescence emission induced by different cations and anions.

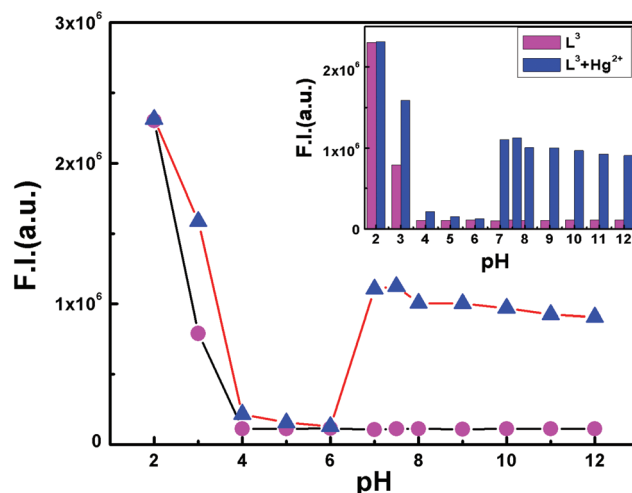


Fig. 4 pH dependent FI of free ligand L^3 (magenta) and the $L^3\text{-Hg}^{2+}$ complex with $L^3:\text{Hg}^{2+} = 1:1.05$ (blue) in the MeCN/H₂O (2:8 v/v) solvent system with $\lambda_{\text{ex}} = 510$ nm. The inset shows the histogram plot.

(Fig. 5) which indicates that L^3 is an ideal chemosensor for Hg^{2+} ions.

Mechanism of ring opening

The characteristic stretching frequency of the amidic “C=O” bond of the rhodamine moiety at 1722 cm^{-1} is shifted to a lower wave number (1633 cm^{-1}) in the presence of 1.2 equiv. of Hg^{2+} (Fig. S2†) indicating a strong polarization of the C=O bond upon efficient binding to the Hg^{2+} ion and, in fact, indicates the cleavage of the N-C bond in the spirolactam ring. Also, the ^1H NMR spectra showed an up-field shift for the azomethine proton mainly due to an increase in electron density arising from the opening of the spirolactam ring.

Steady-state fluorescence studies in the presence of SDS

Steady state fluorescence studies were also carried out in the presence of SDS under two experimental conditions. Firstly, the SDS concentration was kept fixed at 9 mM and $[\text{Hg}^{2+}]$ was varied between 0 and 14 μM keeping $[L^3] = 10\text{ }\mu\text{M}$ (Fig. 6a). A

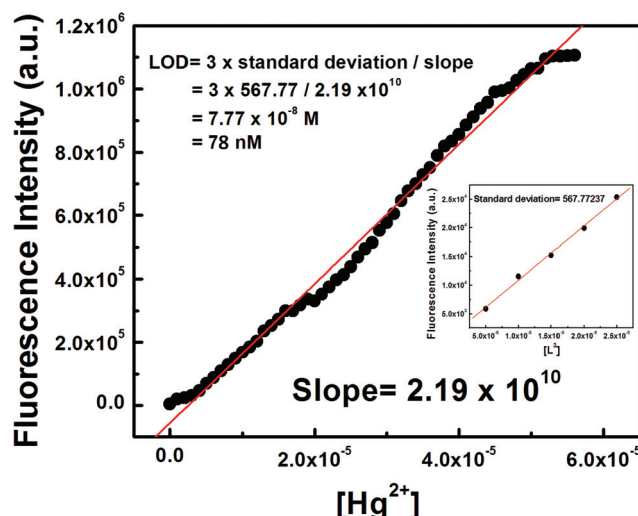


Fig. 5 Determination of the limit of detection (LOD) of Hg^{2+} by L^3 from the slope of the plot of FI vs. $[\text{Hg}^{2+}]$ and the standard deviation of the blank (intercept) determined from the plot of FI vs. $[L^3]$ utilizing the 3σ method.

plot of FI vs. $[\text{Hg}^{2+}]$ resulted in a non-linear curve (Fig. 6b) and was solved by adopting eqn (3). The evaluated K_f value ($4.19 \pm 0.02 \times 10^5\text{ M}^{-1}$) was found to be about one order of magnitude higher than that obtained in the absence of SDS. In order to get the SDS dependent K_f values we have varied $[\text{Hg}^{2+}]$ at different concentrations of SDS and thereby evaluated K_f values were plotted against the concentration of SDS. It was interesting to observe that there is a slow but gradual increase in K_f values with $[\text{SDS}]$ up to 6 mM and further increasing $[\text{SDS}]$ leads to a steep rise in the K_f value up to 9 mM (Fig. 7).

This enhanced stability constant value may be attributed to the restriction to the free dynamic movement of the doubly positively charged $[L^3\text{-Hg}]^{2+}$ complex by the strong electrostatic attraction with the negatively charged head groups of SDS.

Secondly, both $[L^3]$ and $[\text{Hg}^{2+}]$ were kept fixed at 10 μM and $[\text{SDS}]$ was varied between 0 and 10 mM which yielded a non-linear curve on plotting FI vs. $[\text{SDS}]$ showing a plateau at

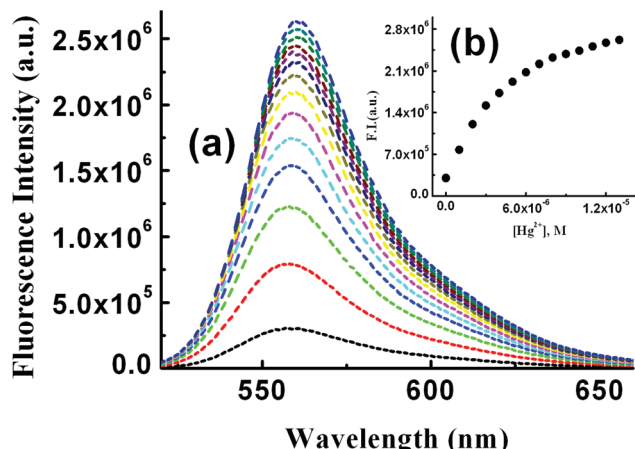


Fig. 6 (a) Fluorescence titration of L^3 as a function of $[\text{Hg}^{2+}]$ at $[\text{L}^3] = 10 \mu\text{M}$ and $[\text{SDS}] = 9.0 \text{ mM}$, in pure water. (b) Plot of FI vs. $[\text{Hg}^{2+}]$.

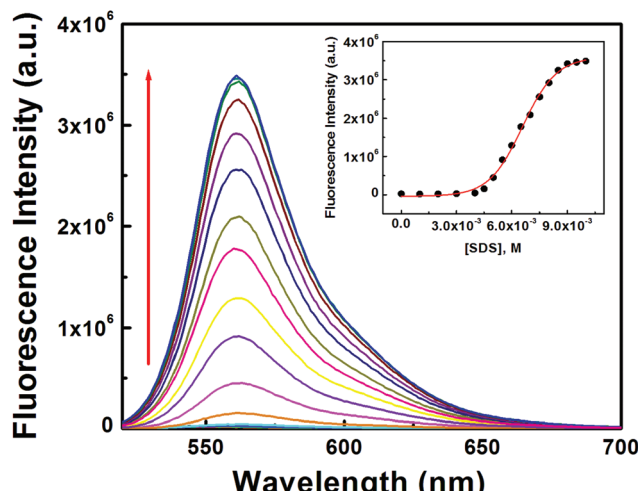


Fig. 8 Fluorescence titration as a function of $[\text{SDS}]$ at $[\text{L}^3] = 10 \mu\text{M}$ and $[\text{Hg}^{2+}] = 10 \mu\text{M}$, in pure water. Inset is the plot of FI vs. $[\text{SDS}]$.

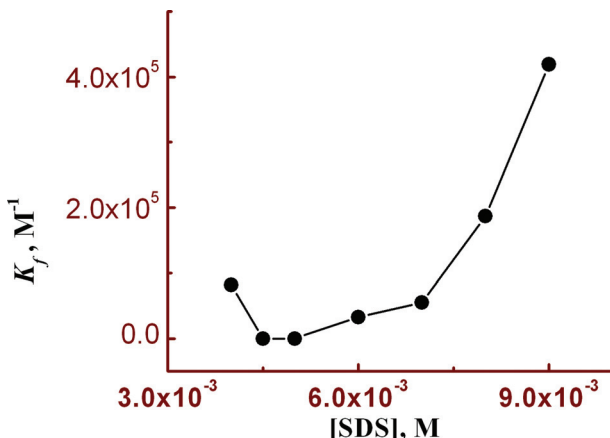


Fig. 7 A plot of K_f as a function of SDS concentration.

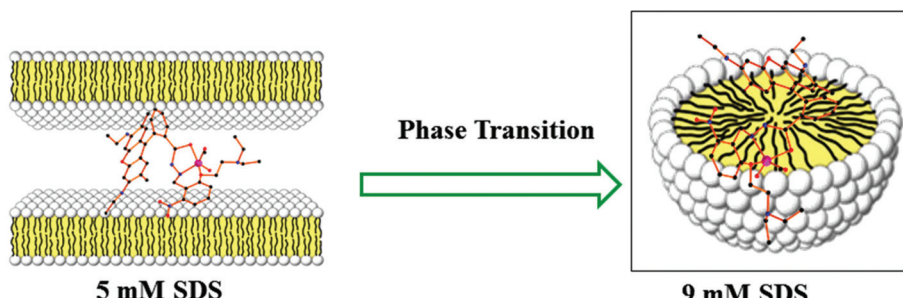
$[\text{SDS}] \sim >9.0 \text{ mM}$ with a fluorescence enhancement of ~ 143 -fold with respect to the complex in the absence of SDS (Fig. 8). The appearance of a plateau at $\sim 9 \text{ mM}$ SDS clearly indicates the critical micellar concentration (CMC) of SDS is $\sim 9.0 \text{ mM}$ under the experimental conditions. The increase in FI with $[\text{SDS}]$ demonstrates aggregation induced enhancement (AIE) of fluorescence. The binding of $\text{L}^3\text{-Hg}^{2+}$ to anionic sulfonic acid groups via electrostatic interactions was confirmed by the failure to observe any change in fluorescence intensity in the presence of cetyltrimethylammonium bromide (CTAB) – a cationic surfactant.

On the basis of these observations, it is concluded that the intermolecular electrostatic interaction between $[\text{L}^3\text{-Hg}^{2+}]$ and SDS may effectively lower the dynamic motion and decrease the non-radiative decay process and hence increase the fluorescence intensity, quantum yield (ϕ) and stability constant (K_f) values compared to the respective values in the absence of SDS.

Steady-state fluorescence anisotropy measurements

Steady-state fluorescence anisotropy can be exploited to get motional information in the micro-heterogeneous environments.⁶² We have monitored the fluorescence anisotropy (r) as a function of SDS concentration (0–10 mM) at a fixed concentration of L^3 and Hg^{2+} (10 μM each) at 553 nm. A plot of r vs. $[\text{SDS}]$ showed a gradual increase in r with $[\text{SDS}]$, reaches a maximum at $\sim 5 \text{ mM}$ and then decreases up to 5.5 and again increases with $[\text{SDS}]$ and becomes constant at $[\text{SDS}] \geq 7.0 \text{ mM}$. This unusual dependence of r on SDS concentration can be rationalized by considering the fact that the initial increase in r is due to trapping of the bi-positive $[\text{L}^3\text{-Hg}^{2+}]$ complex between two co-facial laminar layers which mostly prevailed within 3.0–5.5 mM concentration of SDS (Scheme 2). The decrease in r after 5.0 mM may arise due to phase transition and the second increase in r may be due to the formation of spherical aggregates upon micellization at $\sim 7.0 \text{ mM}$ of SDS and after that the r values become almost constant. The variation of fluorescence anisotropy (r) as a function of SDS concentration is presented in Fig. 9.

To verify whether the probe is trapped inside the hydrophobic core of the micelle or remains in the Stern–Volmer layer we have carried out a fluorescence quenching experiment using EDTA in the presence of SDS at 5 mM and 9 mM concentration and also in the absence of SDS. It was interesting to note that there is no practical quenching of fluorescence intensity of the $\text{L}^3\text{-Hg}^{2+}$ complex on adding 10 equivalents of $\text{H}_2\text{EDTA}^{2-}$ in the presence of 9 mM SDS; however it undergoes a fluorescence quenching by $\sim 50\%$ of its original value in the presence of 5 mM SDS and 100% quenching occurs when there is practically no SDS in the solution (Fig. S7†). All of these observations indicate that the non-accessibility of the $\text{L}^3\text{-Hg}^{2+}$ complexes towards $\text{H}_2\text{EDTA}^{2-}$ is surely due to trapping of $\text{L}^3\text{-Hg}^{2+}$ in the hydrophobic core of the spherical micelle when the SDS concentration is 9 mM. But partial availability of



Scheme 2 Schematic representation of the interactions of $L^3\text{-Hg}^{2+}$ with the laminar microstructure and micellar microstructure of SDS (adopted from <http://fig.cox.miami.edu/~cmallery/255/255chem/mcb2.20.micelle.jpg>).

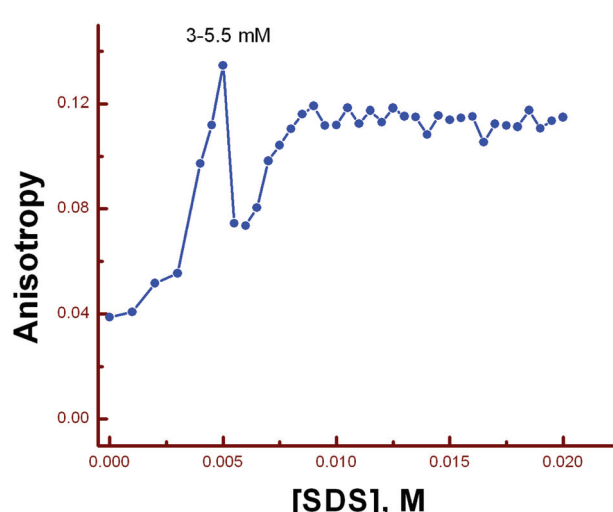


Fig. 9 A plot of anisotropy (r) as a function of SDS concentration.

$L^3\text{-Hg}^{2+}$ towards $\text{H}_2\text{EDTA}^{2-}$ occurs when it is sandwiched in the hydrophilic region between two co-facial laminar layers. We have also carried out SEM and TEM studies on the aggregates at 5.0 mM and 9.0 mM of SDS to support the above proposition and indeed there is some positive indication (Fig. 10 and 11).

SEM and TEM studies

At higher and lower magnifications of the SEM images at 9 mM SDS, a core-shell structure is quite apparent, in which the metallic part is embedded with the ligand and SDS in a definite spherical Janus like structure (Fig. 10). This core-shell structure can also be explained by the TEM studies; the inner core (dark black) of the particle is comprised of the metallic zone (Fig. 11) and the outer shell is the ligand along with SDS which are in agglomerated conditions due to the hydrophilic interactions. However, in the presence of 5 mM SDS the probe undergoes extensive aggregation with no definite shape which is also prevailing from both the SEM and TEM studies.

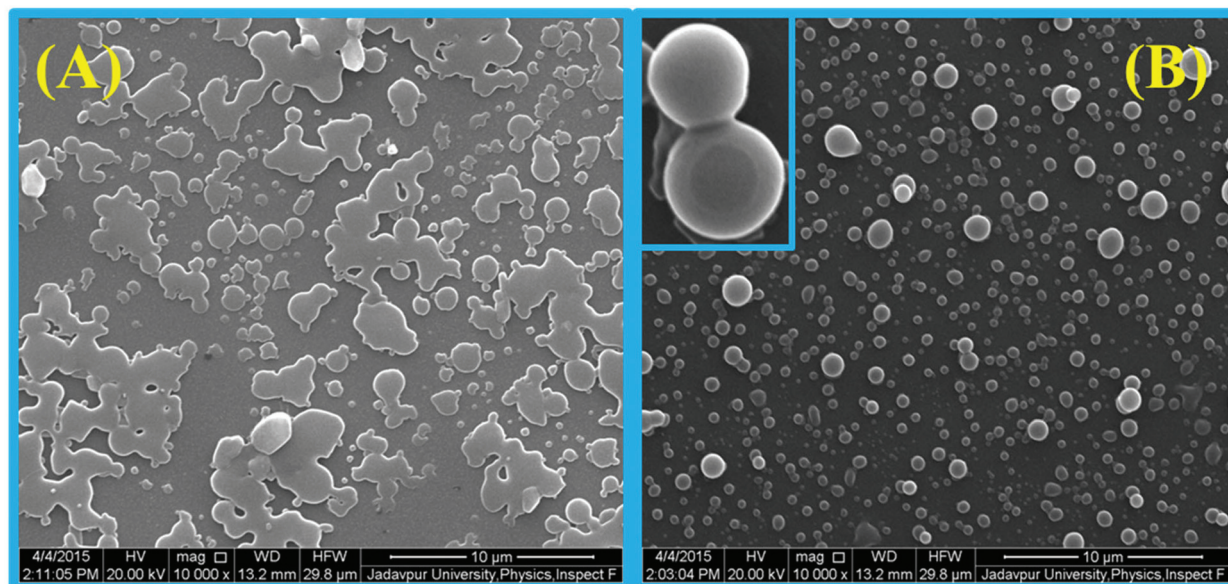


Fig. 10 SEM images of L^3 (10 μM)- Hg^{2+} (10 μM) in the presence of (A) 5.0 mM SDS showing an agglomerated microstructure with no particular shape and (B) 9.0 mM SDS with a spherical microstructure.

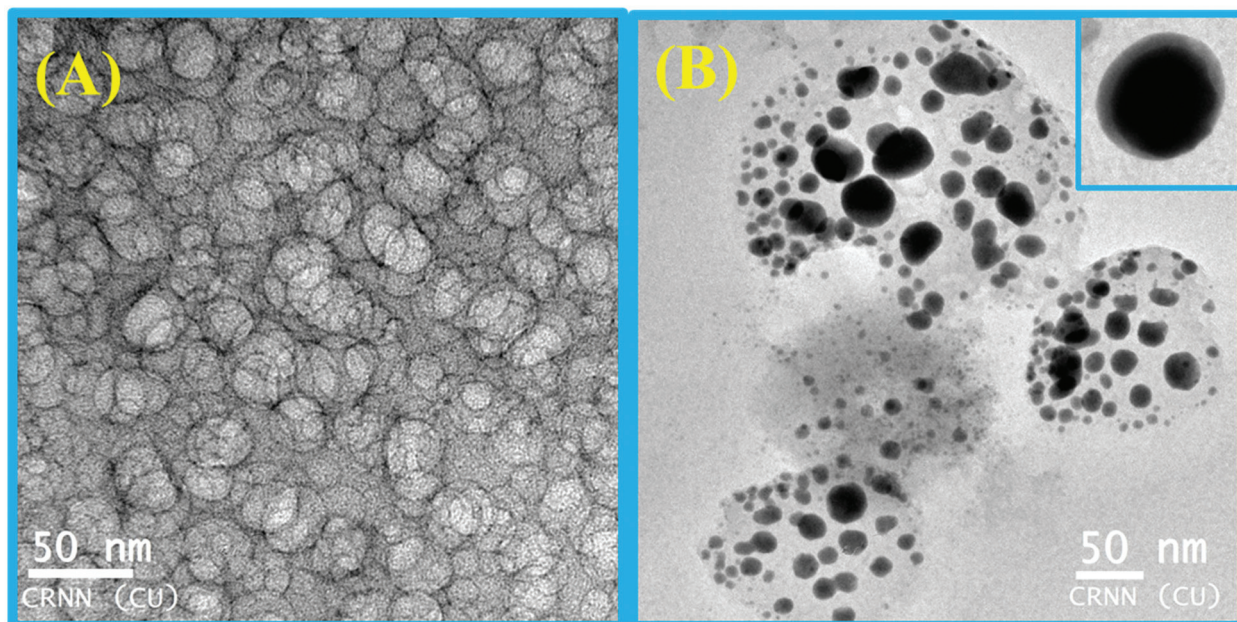


Fig. 11 TEM images of $\text{L}^3\text{-Hg}^{2+}$ in the presence of (A) 5.0 mM SDS and (B) 9.0 mM SDS.

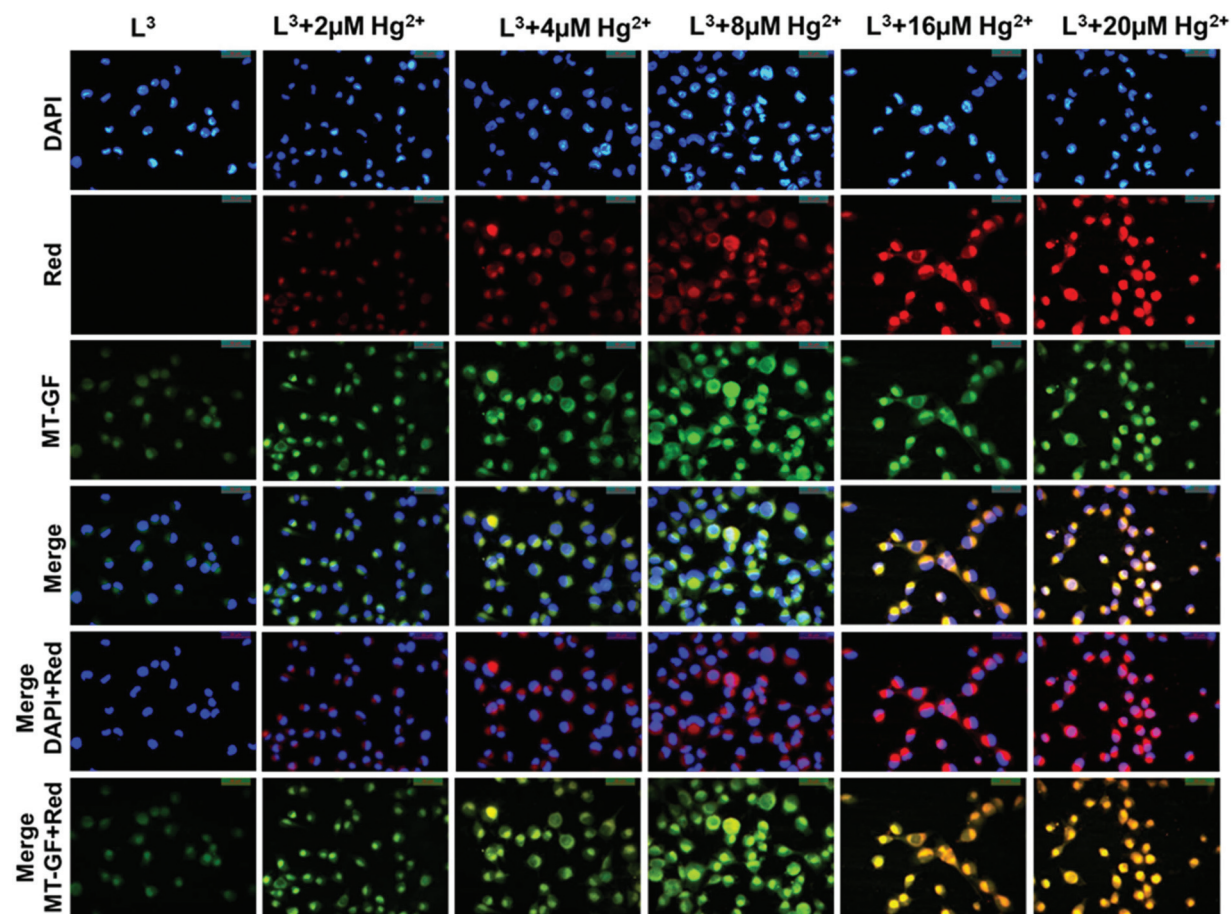


Fig. 12 Cell imaging studies of Hg^{2+} ions with L^3 . The fluorescence images of the HepG2 cells were captured (40 \times) after incubation with 10 μM L^3 for 30 min at 37 °C and pre-incubation with (2, 4, 8, 16 and 20 μM) Hg^{2+} for 3 h at 37 °C followed by washing thrice with 1x PBS. The images show strong cytoplasmic red fluorescence when L^3 complexes with Hg^{2+} (red). The merged images show that the $\text{L}^3\text{-Hg}^{2+}$ fluorescence is cytoplasmic and not in the nucleus. Cytoplasmic complex formation was confirmed using DAPI (nuclear stain, blue) and MitoTracker Green FM (MT-GF, cytoplasm stain, green).

Cell studies

Mitochondria are cytoplasmic organelles in the eukaryotic cell and produce ATP (95%) required for the cell. In nerve cells mitochondrial function has a very crucial role to meet the high, long term and specific energy demand to regulate brain functions. The basic mechanism for mercury toxicity emerges from the direct and indirect damage of mitochondria through reduction of glutathione due to extreme ROS (reactive organic species) generation and increased mitochondrial membrane permeability. Hence, there is a certain need to detect Hg^{2+} in its permissible limits to avoid its toxicity and also to apply a chelator based treatment to reduce Hg^{2+} poisoning in humans. In the present study we evaluate the chemosensing capability of L^3 to detect Hg^{2+} . The cytotoxic effects of L^3 were determined by a cell viability assay in HepG2 cells. Up to 50 μM shows less than 30% cytotoxicity for L^3 and more than 87% of cells are viable up to a dose of 20 μM (Fig. S8†). Hence no significant cytotoxicity was observed up to 20 μM . Furthermore, we have assessed the Hg^{2+} ion detection capability of L^3 using *in vitro* fluorescence analysis in HepG2 cells (Fig. 12). Intracellular imaging of HepG2 cells treated with the L^3 ligand (10 μM) reveals no intracellular fluorescence. Yet, live cell imaging of HepG2 cells treated with equimolar amounts of Hg^{2+} and the L^3 ligand shows excellent intracellular cytoplasmic red fluorescence (Fig. 12).

A concentration dependent increase in the red fluorescence was noted indicating L^3 as an excellent cytoplasmic Hg^{2+} tracker. We have observed that L^3 can sense low concentrations of Hg^{2+} ions present in the cytoplasm (2–8 μM). We didn't see any nuclear binding of $\text{Hg}^{2+}\text{--L}^3$; this may be due to the restricted permeability of L^3 to the cytoplasm (Fig. 12). Hence the presented ligand has low cytotoxicity and is biocompatible for cellular cytoplasmic Hg^{2+} ion detection and can be used for Hg^{2+} ion detection in biological samples.

Conclusion

A new type of easily synthesized rhodamine-based chemosensor with potential NO_2 donor atoms showed selective and rapid recognition of toxic Hg^{2+} ions. The binding stoichiometry of the sensor with Hg^{2+} was established by the combined Job's and HRMS (*m/z*) methods. All biologically relevant metal ions as well as toxic heavy metal ions and anions did not interfere with the detection of Hg^{2+} ions. The detection limit of Hg^{2+} calculated using the 3σ method gives a value of 78 nM. Bio-compatibility and good solubility in a mostly aqueous medium (8 : 2, $\text{H}_2\text{O}:\text{MeCN}$) along with its cell permeability with no or negligible cytotoxicity indicate good potential for *in vitro/in vivo* cell imaging studies which showed cytoplasmic recognition of Hg^{2+} ions. Under an optical microscope, a heavily agglomerated microstructure of $\text{L}^3\text{--Hg}^{2+}$ in 5 mM SDS changes to a spherical shape in 9 mM SDS. Not only that, we have also carried out fluorescence titrations in the presence of SDS and also the SDS concentration was varied at a fixed concentration of the receptor and the guest. The

presence of SDS causes an enhanced quantum yield (ϕ) and more importantly the stability constant (K_f) by ~an order of magnitude compared to those in the absence of SDS. Again, the FI of the $[\text{L}^3\text{--Hg}]^{2+}$ complex is enhanced by 143 fold compared to that in the absence of SDS. So an attempt was made to get some idea of the dependence of K_f on SDS concentration. It was interesting to see that a plot of K_f as a function of [SDS] showed an initial slow increase in K_f up to 6 mM of SDS and then it picked up rapidly indicating the occurrence of aggregation induced emission enhancement (AIEE). All of these observations clearly manifest in an enhanced rigidity of the $[\text{L}^3\text{--Hg}]^{2+}$ complex in the heterogeneous micro-environment restricting the dynamic movement of the $[\text{L}^3\text{--Hg}]^{2+}$ complex. The change in fluorescence anisotropy (r) with [SDS] is best described by a change in the morphology of the SDS microstructure from laminar to a spherical shape; the former being more efficient to provide better rigidity to the $[\text{L}^3\text{--Hg}]^{2+}$ complex and hence higher r values at ~5 mM of SDS.

Acknowledgements

Financial support from the Department of Science and Technology (DST), Government of India, New Delhi (ref. number SR/S1/IC-20/2012) is gratefully acknowledged. Instrumental facilities FE-SEM from the Department of Physics (DST-FIST) Jadavpur University and TEM from the CRNN, University of Calcutta are gratefully acknowledged.

Notes and references

- 1 S. Zhang, *Nat. Biotechnol.*, 2003, **21**, 1171–1178.
- 2 L. Wang, L. L. Li, H. L. Ma and H. Wang, *Chin. Chem. Lett.*, 2013, **24**, 351–358.
- 3 T. L. Greaves and C. J. Drummond, *Chem. Soc. Rev.*, 2013, **42**, 1096–1120.
- 4 T. Y. Ma, H. Li, Q. F. Deng, L. Liu, T. Z. Ren and Z. Y. Yuan, *Chem. Mater.*, 2012, **24**, 2253–2255.
- 5 C. Lv, G. Xu and X. Chen, *Chem. Lett.*, 2012, **41**, 1201–1203.
- 6 A. M. Perceboom, J. Janiak, K. Schillén, L. Piculell and W. Loh, *Soft Matter*, 2013, **9**, 515–526.
- 7 Y. N. Guo, Y. Li, B. Zhi, D. Zhang, Y. Liu and Q. Huo, *RSC Adv.*, 2012, **2**, 5424–5429.
- 8 L. G. Chen and H. Bermudez, *Langmuir*, 2012, **28**, 1157–1162.
- 9 S. L. de-Rooy, S. Das, M. Li, B. El-Zahab, A. Jordan, R. Lodes, A. Weber, L. Chandler, G. A. Baker and I. M. Warner, *J. Phys. Chem. C*, 2012, **116**, 8251–8260.
- 10 Y. Liu, X. Feng, J. Shi, J. Zhi, B. Tong and Y. Dong, *Chin. J. Polym. Sci.*, 2012, **30**, 443–450.
- 11 Y. Ren and T. Baumgartner, *Inorg. Chem.*, 2012, **51**, 2669–2678.
- 12 X. Chen, Y. Xiang, P. Song, R. Wei, Z. Zhou, K. Li and A. Tong, *J. Lumin.*, 2011, **131**, 1453–1459.
- 13 B. Xu, Z. Chi, X. Li, H. Li, W. Zhou, X. Zhang, C. Wang, Y. Zhang, S. Liu and J. Xu, *J. Fluoresc.*, 2011, **21**, 433–441.

- 14 E. Lucenti, C. Botta, E. Cariati, S. Righetto, M. Scarpellini, E. Tordin and R. Ugo, *Dyes Pigm.*, 2013, **96**, 748–755.
- 15 C. Shi, Z. Guo, Y. Yan, S. Zhu, Y. Xie, Y. S. Zhao, W. Zhu and H. Tian, *ACS Appl. Mater. Interfaces*, 2013, **5**, 192–198.
- 16 P. Guo, S. Yan, Y. Zhou, C. Wang, X. Xu, X. Weng and X. Zhou, *Analyst*, 2013, **138**, 3365–3367.
- 17 W. Z. Yuan, Z. Q. Yu, P. Lu, C. Deng, J. W. Y. Lam, Z. Wang, E. Q. Chen, Y. Mad and B. Z. Tang, *J. Mater. Chem.*, 2012, **22**, 3323–3326.
- 18 G. Yu, S. Yin, Y. Liu, J. Chen, X. Xu, X. Sun, D. Ma, X. Zhan, Q. Peng, Z. Shuai, B. Z. Tang, D. Zhu, W. Fang and Y. Luo, *J. Am. Chem. Soc.*, 2005, **127**, 6335–6346.
- 19 X. Gu, J. Yao, G. Zhang, C. Zhang, Y. Yan, Y. Zhao and D. Zhang, *Chem. – Asian J.*, 2013, **8**, 2362–2369.
- 20 J. Luo, X. Wang, X. Wang and W. Su, *Chin. J. Chem.*, 2012, **30**, 2488–2494.
- 21 X. Zhou, H. Li, Z. Chi, B. Xu, X. Zhang, Y. Zhang, S. Liu and J. Xu, *J. Fluoresc.*, 2012, **22**, 565–572.
- 22 W. Wu, S. Ye, R. Tang, L. Huang, Q. Li, G. Yu, Y. Liu, J. Qin and Z. Li, *Polymer*, 2012, **53**, 3163–3171.
- 23 B. K. An, S. K. Kwon, S. D. Jung and S. Y. Park, *J. Am. Chem. Soc.*, 2002, **124**, 14410–14415.
- 24 S. J. Li, B. K. An, S. D. Jung, M. A. Chung and S. Y. Park, *Angew. Chem., Int. Ed.*, 2004, **43**, 6346–6350.
- 25 J. B. Birks, *Photophysics of Aromatic Molecules*, Wiley, London, 1970.
- 26 X. Cao, R. W. Tolbert, J. L. McHale and W. D. Edwards, *Dye J. Phys. Chem. A*, 1998, **102**, 2739–2748.
- 27 R. Badugu, J. R. Lakowicz and C. D. Geddes, *J. Am. Chem. Soc.*, 2005, **127**, 3635–3641.
- 28 Y. Ren, J. W. Y. Lam, Y. Dong, B. Z. Tang and K. S. Wong, *J. Phys. Chem. B*, 2005, **109**, 1135–1140.
- 29 H. Tong, Y. Dong, Y. Hong, M. Haussler, J. W. Y. Lam, H. H. Y. Sung, X. Yu, J. Sun, I. D. Williams, H. S. Kwok and B. Z. Tang, *J. Phys. Chem. C*, 2007, **111**, 2287–2294.
- 30 Z. Li, Y. Dong, B. Mi, Y. Tang, M. Haussler, H. Tong, Y. Dong, J. W. Y. Lam, Y. Ren, H. H. Y. Sung, K. S. Wong, P. Gao, I. D. Williams, H. S. Kwok and B. Z. Tang, *J. Phys. Chem. B*, 2005, **109**, 10061–10066.
- 31 L. S. Hung and C. H. Chen, *Mater. Sci. Eng.*, 2002, **39**, 143–222.
- 32 J. H. Burroughes, D. D. C. Bradley, A. R. Brown, R. N. Marks, K. Mackay, R. H. Friend, P. L. Burns and A. B. Holmes, *Nature*, 1990, **347**, 539–541.
- 33 J. Chen, C. C. W. Law, J. W. Y. Lam, Y. Dong, S. M. F. Lo, I. D. Williams, D. Zhu and B. Z. Tang, *Chem. Mater.*, 2003, **15**, 1535–1546.
- 34 M. Rosoff, *Ed. Vesicles*, Dekker, New York, 1996.
- 35 C. F. J. Faul, *Adv. Mater.*, 2003, **15**, 673–683.
- 36 P. Bilski, R. N. Holt and C. F. Chignell, *J. Photochem. Photobiol. A*, 1997, **110**, 67–74.
- 37 P. Bilski and C. F. Chignell, *J. Photochem. Photobiol. A*, 1994, **77**, 49–58.
- 38 H. Hachisako and R. Murakami, *Chem. Commun.*, 2006, 1073–1075.
- 39 H. Hachisako, N. Ryu and R. Murakami, *Org. Biomol. Chem.*, 2009, **7**, 2327–2337.
- 40 A. K. Chibisov, V. I. Prokhorenko and H. Görner, *Chem. Phys.*, 1999, **250**, 47–60.
- 41 A. K. Mandal and M. K. Pal, *Chem. Phys.*, 2000, **253**, 115–124.
- 42 L. Tang, J. Jin, S. Zhang, Y. Mao, J. Sun, W. Yuan, H. Zhao, H. Xu, A. Qin and B. Tang, *Sci. China, Ser. B: Chem.*, 2009, **52**, 755–759.
- 43 Y. F. Zhang, Q. Yuan, T. Chen, X. B. Zhang, Y. Chen and W. H. Tan, *Anal. Chem.*, 2012, **84**, 1956–1962.
- 44 E. S. Childress, C. A. Roberts, D. Y. Sherwood, C. L. M. LeGuyader and E. J. Harbron, *Anal. Chem.*, 2012, **84**, 1235–1239.
- 45 L. Deng, X. Y. Ouyang, J. Y. Jin, C. Ma, Y. Jiang, J. Zheng, J. S. Li, Y. H. W. Li, H. Tan and R. H. Yang, *Anal. Chem.*, 2013, **85**, 8594–8600.
- 46 P. B. Tchounwou, W. K. Ayensu, N. Ninashvili and D. Sutton, *Environ. Toxicol.*, 2003, **18**, 149–175.
- 47 V. D. Bittner Jr., J. S. Echeverria, H. V. Woods, C. Aposhian, M. D. Naleway, R. K. Martin, N. J. Mahurin and M. Cianciola, *Neurotoxicol. Teratol.*, 1998, **20**, 429–439.
- 48 F. Di Natale, A. Lancia, A. Molino, M. Di Natale, D. Karatza and D. Musmarra, *J. Hazard. Mater.*, 2006, **132**, 220.
- 49 Y. Gao, S. De Galan, A. DeBauwere, W. Baeyens and M. Leermakers, *Talanta*, 2010, **82**, 1919–1923.
- 50 F. Moreno, T. Garcia-Barrera and J. L. Gomez-Ariza, *Analyst*, 2010, **135**, 2700–2705.
- 51 X. Chai, X. Chang, Z. Hu, Q. He, Z. Tu and Z. Li, *Talanta*, 2010, **82**, 1791–1796.
- 52 X. Fu, X. Chen, Z. Guo, C. Xie, L. Kong, J. Liu and X. Huang, *Anal. Chim. Acta*, 2011, **685**, 21–28.
- 53 J. R. Lakowicz, *Principles of Fluorescence Spectroscopy*, Springer, New York, 3rd edn, 2006, p. 67.
- 54 R. P. Haugland, *The Handbook: A Guide to Fluorescent Probes and Labeling Technologies*, Invitrogen Corp., Carlsbad, CA, 10th edn, 2005.
- 55 H. Y. Lee, K. M. K. Swamy, J. Y. Jung, G. Kim and J. Yoon, *Sens. Actuators, B*, 2013, **182**, 530–537.
- 56 F. Wang, S. W. Nama, Z. Guo, S. Parka and J. Yoona, *Sens. Actuators, B*, 2012, **161**, 948–953.
- 57 X. Chen, T. Pradhan, F. Wang, J. S. Kim and J. Yoon, *Chem. Rev.*, 2012, **112**, 1910–1956.
- 58 K. Bera, A. K. Das, M. Nag and S. Basak, *Anal. Chem.*, 2014, **86**, 2740–2746.
- 59 V. Dujols, F. Ford and A. W. Czarnik, *J. Am. Chem. Soc.*, 1997, **119**, 7386–7387.
- 60 R. P. Haugland, *The Handbook: A Guide to Fluorescent Probes and Labeling Technologies*, Invitrogen Corp., Carlsbad, CA, 10th edn, 2005.
- 61 L. Huang, X. Wang, G. Xie, P. Xi, Z. Li, M. Xu, Y. Wu and D. Baib, *Dalton Trans.*, 2010, **39**, 7894–7896.
- 62 R. Bhowmick, R. Alam, T. Mistri, D. Bhattacharya, P. Karmakar and M. Ali, *Appl. Mater. Interfaces*, 2015, **7**, 7476–7485.
- 63 C. R. Lohani, J. M. Kim, S. Y. Chung, J. Yoon and K. H. Lee, *Analyst*, 2010, **135**, 2079–2084.